Available online at www.sciencedirect.com

ScienceDirect

journal homepage: www.elsevier.com/locate/he

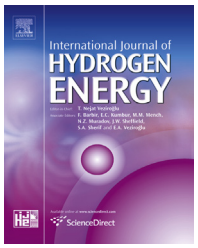

Role of crystallographic texture on the improvement of hydrogen-induced crack resistance in API 5L X70 pipeline steel

Mohammad Masoumi [a,*], *Cleiton Carvalho Silva* [a], *Miloslav Béreš* [a], *Duberney Hincapie Ladino* [b], *Hamilton Ferreira Gomes de Abreu* [a]

[a] *Federal University of Ceará, Department of Metallurgical and Materials Engineering, Campus do Pici, Bloco 729, CEP 60.440-554, Fortaleza, Ceará, Brazil*

[b] *University of São Paulo, Department of Metallurgical and Materials Engineering, Av. Prof. Mello Moraes, 2463, 05508-030, São Paulo, SP, Brazil*

ARTICLE INFO

Article history:
Received 3 July 2016
Received in revised form
20 October 2016
Accepted 21 October 2016
Available online 10 November 2016

Keywords:
API 5L X70
Hydrogen-induced cracking
Rolling temperature
Texture

ABSTRACT

The purpose of this work was to improve the resistance of hydrogen-induced cracking in API 5L X70 steel by engineering the crystallographic texture and grain boundary distributions via different rolling temperatures. Hydrogen-induced cracking and electrochemical hydrogen charging tests were carried out in two different conditions: commercially produced and isothermally rolled at 850 °C in laboratory. The results showed that the development of dominant {011} grains parallel to the normal direction, and a small number of {001}//ND grains obtained by isothermal rolling at 850 °C, increased the hydrogen-induced crack resistance; while the hot rolled sample with sharp {001}//ND textures was highly susceptible to cracking.

Introduction

American Petroleum Institute (API) steels have attracted considerable attention due to the low content of carbon and other alloying elements, economic fabrication and easy installation. These steels are widely used for transportation of natural gas and crude oil across long distances [1,2]. Hydrogen-induced cracking (HIC) is considered as the main damage mode in the sour environment (i.e. containing water and H_2S) and causes huge economic loss [1–3]. Atomic hydrogen produced during surface pipe corrosion diffuses into the steel and traps at defect sites such as inclusions, precipitations, phase interfaces, martensite islands, and grain boundaries. These hydrogen atoms recombine to form hydrogen molecules, leading to the creation of internal pressure within the metal. This reduces ductility, toughness, and mechanical properties, called hydrogen embrittlement [3,4].

The HIC behaviour depends on many metallurgical factors such as chemical composition, segregation, microstructure, inclusions and microstructural defects [5,6]. In addition, the effect of crystallographic texture on HIC susceptibility was also studied in the last decade [7–9]. However, the effects of engineering the crystallographic texture and grain boundary

* *Corresponding author.*
E-mail address: mohammad@alu.ufc.br (M. Masoumi).
http://dx.doi.org/10.1016/j.ijhydene.2016.10.124

orientation on improving HIC resistance has not been employed in pipe manufacturing. The mechanism of HIC at the crystal scale is described by hydrogen-enhanced decohesion (HEDE), absorption-induced dislocation emission (AIDE), and hydrogen-enhanced plasticity (HELP) theories [10,11]. HEDE is related to increasing internal pressure at trap sites due to the recombination of hydrogen molecules leading to crack nucleation. Next, AIDE is associated with cleavage-like fracture in low resistance paths to release the energy. Finally, HELP is associated with a lack of sufficient slip systems, facilitating crack growth and propagation in material.

It is well known that the preferred crystallographic texture that develops during the manufacturing process influence the final properties. Wright and Field [12] confirmed the feasibility of improving mechanical properties and corrosion resistance of steels by controlling crystallographic textures and grain boundary engineering. Masoumi et al. [13,14] and Nafisi et al. [15] reported that controlled warm rolling– between half of the melting point and the non-recrystallisation temperature (T_{NR}) – produces {111}//ND and {110}//ND dominant crystallographic textures in API steel. Venegas et al. [7] reported that the large proportion of grains oriented with {001} planes parallel to normal direction {001}//ND promote intergranular crack propagation, leading to a reduction of HIC resistance. In contrast, the well-developed {112}//ND and {111}//ND fibre textures with small fraction of {001}//ND texture enhanced the HIC resistance [7–9]. Contrary to these findings, Mohtadi-Bonab et al. [9,10] reported that there is no preferred direction for HIC propagation, while other crystallographic factors such as grain boundary characteristics, the distribution of recrystallised grains and the Taylor factor distribution can play significant roles in governing the HIC behaviour. In addition, it was also shown that transgranular cracks propagate in grains with high Taylor factor, whereas intergranular cracks occur where a mismatch in Taylor factor between neighbouring grains exists [16]. The current work aims to clarify the above mentioned contrasting results and show the effect of engineering of crystallographic texture on HIC behaviour.

Here, we present the role of macrotexture, microtexture, and mesotexture[1] on HIC susceptibility in API X70 steel as a strong candidate in the sour service environment. In this respect, at first favourable crystallographic textures (i.e. {111}// ND and {110}//ND) were produced by isothermal rolling at 850 °C and compared to that in commercially available steel. The microstructural and textural evolution was characterised by scanning electron microscopy (SEM), X-ray diffraction (XRD) and electron backscatter diffraction (EBSD). Samples were subjected to both HIC test and electrochemical hydrogen charging test to evaluate the effect of distinct crystallographic texture which was produced by different thermomechanical treatments on cracking behaviour. Then EBSD analysis was carried out to find a correlation between HIC behaviour (i.e. nucleation and propagation), microstructure and crystallographic orientation. Present work revealed that significant improving of HIC resistance was obtained through engineering of crystallographic texture by isothermal rolling below non-recrystallisation temperature. The high resistance to HIC is highly important to oil and gas transportation.

[1] The terms macrotexture, microtexture, and mesotexture refer to the average sample texture, the crystallographic orientation of a microstructure point, and the texture of grain boundaries, respectively.

Experimental details

A commercial API 5L X70 steel as a typical grade used for the manufacturing of pipelines transporting oil and gas in Brazil was studied in this work and its chemical composition is listed in Table 1. Higher molybdenum content in the investigated steel (i.e. 0.8 wt.-%) significantly increases the pitting and naphthenic corrosion resistance [17] which is the main challenge of offshore pipeline in Brazil.

The material was delivered in form of 9 mm thick plate. The plate was cut into two sections; each was subjected to the same rolling schedule however at different temperatures. The first section was rolled in the recrystallisation austenite region ($T_{NR} = 1006$ °C: [18]) at around 1200 °C (designated as hot rolled sample), while the other was isothermally rolled in the non-recrystallisation austenite field at 850 °C (designated as warm rolled sample). For the rolling a Stanat model TA-315 rolling machine was used with 273 rpm rotational speed, in three passes to reach 3 mm thickness (9 mm → 7 mm → 5 mm → 3 mm), followed by air cooling to room temperature. The main reason for the selection of different temperatures above and below the non-recrystallisation temperature was to characterise the effect of recrystallisation on textural evolution and its effect on HIC susceptibility.

To estimate the HIC resistance, two samples of each specimen were cut and prepared from the mid-thickness of rolling plane, considered as the most susceptible region to the HIC test plane. The mid-thickness of the pipeline is considered as the most susceptible region to the HIC due to the segregation of alloying elements (i.e. manganese and carbon) in this region. This leads to the formation of hard microconstituents which promote nucleation and propagation of the cracks [1–4]. The samples were then ground using 1200 grit paper, then polished with 6, 3 and 1 μm diamond paste. Next, the samples were embedded in resin with a copper wire for electric contact. 0.2 M sulphuric acid (H_2SO_4) aqueous solution was used for electrochemical hydrogen charging. Moreover, to prevent the formation of hydrogen bubbles on the surface of the specimen and to increase the amount of hydrogen entering the steel, 3 g/l arsenic trioxide (As_2O_3) was added to the solution. Finally, each sample was electrochemically charged for 6 h with a constant current of 20 mA/cm^2 [19]. Fig. 1 shows that the current density of 20 mA/cm^2 corresponds to a cathodic potential of 0.7 V_{SCE}. In addition, HIC resistance was evaluated according to NACE TM0284-2011 standard [20] on samples charged for 96 h at 25 °C. The test solution consisted of 5.0 wt. % NaCl and 0.5 wt. % CH_3COOH in distilled water saturated with H_2S at 1 bar. The initial and final pH values of the solution were 2.7 and 3.1, respectively. Fig. 2 shows schematic plot of the HIC procedure.

Microstructural studies were carried out along the rolling plane of the samples, using scanning electron microscopy (SEM). The rolled samples were prepared by grinding with SiC papers up to 1200 grit and then polishing with 6, 3 and 1 μm

Table 1 – Chemical composition of API 5L X70 steel (in wt. -%).

C	Si	Mn	S	Al	Cu	Cr	P
0.099	0.259	1.664	0.006	0.042	0.014	0.021	0.018
Ni	Mo	Nb	Ti	V	Ni + V + Ti	CE_{Pcm}	CE_{IIW}
0.022	0.816	0.062	0.019	0.050	0.131	0.203	0.409

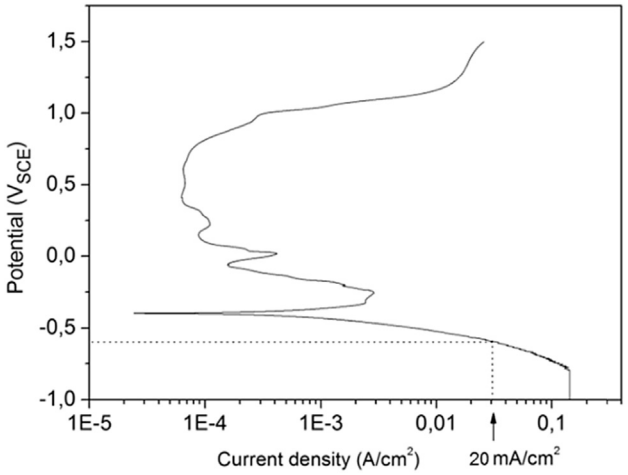

Fig. 1 – Electrochemical test showing that current density of 20 mA/cm² corresponds to a cathodic potential of 0.7 V_{SCE}.

diamond paste. Finally, the specimens were etched with 2% nital solution for approximately 40 s. The Vickers hardness was measured in the aforementioned regions of the samples.

Macrotextural characterisations were measured by X'Pert X-ray diffractometers equipped with Philips texture goniometer on rolling plane. Three incomplete pole figures, i.e., {110}, {200}, and {211} were obtained, using Cr radiation, in the reflection mode on a 5° step up to 85° sample tilt. The orientation distribution function (ODF) of each sample was calculated from the measured pole figures using MTEX-free and open source software toolbox. The $\varphi_2 = 45°$ section of Euler space was used to display the computed ODFs. Furthermore, EBSD analysis was conducted in the RD-ND plane of the investigated samples using FEI Quanta FEG 450 scanning electron microscope operating at an acceleration voltage of 20 kV, sample tilt angle of 70°, working distance of 12 mm and 0.5 μm step size. The Channel 5 and MTEX software were used to analyse and display results.

Results and discussion

The SEM micrographs obtained from the rolling plane (RD-TD section) of both hot and warm rolled samples are shown in Fig. 3. The first sample, which was rolled industrially at about 1200 °C, showed a banded ferrite-pearlite microstructure, which is common in hot rolled conditions (Fig. 3a). Moreover, the hardness and ferrite grain sizes were 165 ± 5 HV and 8 ± 1 μm, respectively. Martensite-austenite (M/A) constituents dispersed on ferritic microstructure were observed in the warm rolled sample (Fig. 3b). It is to be noted that no pearlite was found in this sample. Zhu et al. [21] reported that carbon and other alloying elements that were drawn back due to the nucleation of ferrite from the prior austenite grain boundaries led to the formation carbides and M/A constituents. Moreover, their uniform distribution strongly increases the impact toughness and strength [17]. In the present work also pancake-shaped austenite grains formed during rolling below the non-recrystallisation temperature which increased the number of ferrite nucleation sites. In this condition, the hardness and ferrite grain sizes were 198 ± 5 HV and 6 ± 0.7 μm, respectively. It is worth mentioning that no segregation zone was found in both samples.

Fig. 4 shows the calculated ODF at $\varphi_2 = 45°$ of the rolled samples. In the hot rolled sample the rotated cube (001)<110>

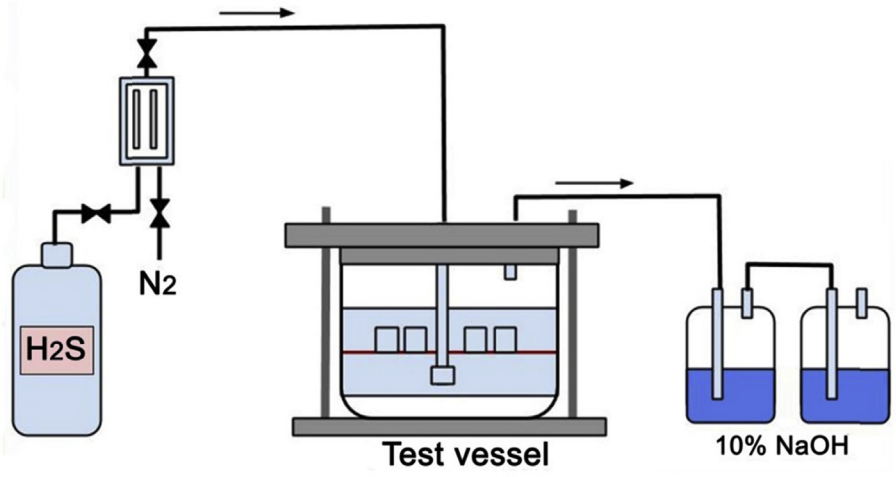

Fig. 2 – Schematic plot used for hydrogen induced cracking test.

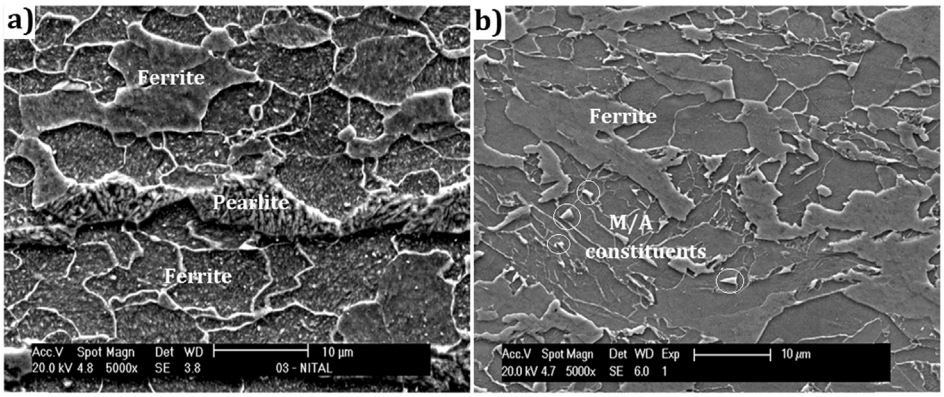

Fig. 3 – SEM micrographs of a) hot and b) warm rolled sample.

texture components were dominant (Fig. 4a). Zhang et al. [22] reported the formation of strongly rotated cube texture components generated from recrystallisation of austenite grains at higher annealing temperatures, followed by ferrite transformation during cooling, which is in agreement with our result. On the other hand, the warm rolled sample demonstrated a strong {110}//ND fibre with predominant (110)[1$\bar{1}$ 3] texture component which is deflected about 10° from the Goss orientation (110)[001] component. The shear deformation caused by the friction between the rolls and sheet surface could develop {110}//ND crystallographic textures [23]. Moreover, to illustrate the effect of rolling temperature on the texture evolution, skeleton plots for main fibres including α-fibre {001}//RD, γ-fibre {111}//ND in addition to {001}//ND and {110}//ND texture components were plotted and these are presented in Fig. 5. Fig. 5a and b shows that warm rolling decreased the fraction of undesirable {001} oriented grains which can cause an increase in HIC resistance. There is no significant difference in {111}//ND texture components in both hot and warm rolled sample, Fig. 5c. However, an extensive increase in intensity of {110}//ND texture was observed in warm rolled sample, Fig. 5d.

The typical stepwise hydrogen-induced crack in hot rolled steel is shown in Fig. 6. The crack is parallel to the rolling direction with some deflections towards the normal direction. In the warm rolled sample, no crack was found (not shown here). The difference in the HIC resistance in the examined samples might be explained by the formation of different microstructural constituents in the specimens. As mentioned earlier, in the hot rolled specimen, ferrite-pearlite microstructure with relatively large grain size developed and HIC crack tended to nucleate and propagate along ferrite-pearlite interfaces. It is to be noted that SEM analysis did not revealed any inclusions in the vicinity of cracks. In contrast, the warm rolled steel presented fine ferritic microstructure with M/A and cementite constituents, formed at lower rolling temperatures and exhibited higher resistance to HIC propagation.

Non-metallic inclusions such as MnS can play a significant role in HIC initiation and high amount of sulphur content in the steel probably led to development of these inclusions, no inclusions were found in the vicinity of crack path. Although there is a possibility of forming inclusions in the steel, determination of its content (i.e. using ASTM E45) was not focus of the study present.

In order to investigate the role of crystallographic orientation and grain boundary distributions on HIC behaviour, EBSD analysis was conducted in the vicinity of the hydrogen crack with no presence of pearlite. Fig. 7 presents the inverse pole figure (IPF) map in the vicinity of HIC. In this figure low-angle grain boundaries- LAGBs (point-to-point misorientations less than 15°) and high-angle grain boundaries-

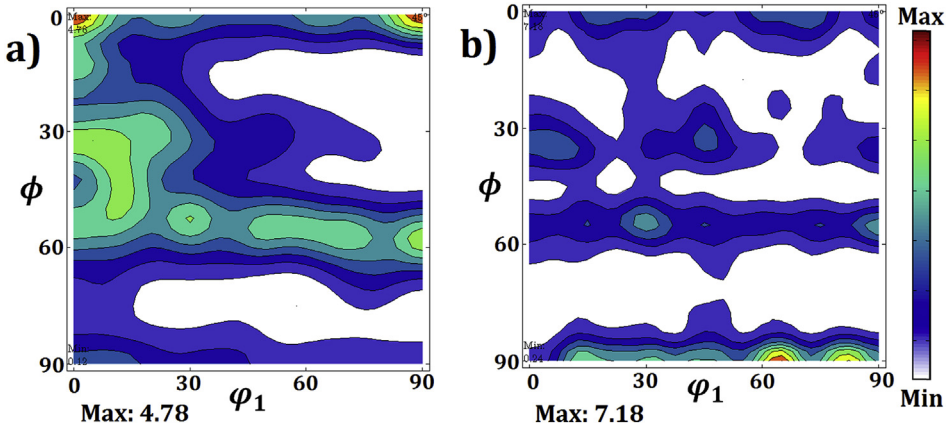

Fig. 4 – Texture components in a constant $\varphi_2 = 45°$ section of the ODF of a) hot and b) warm rolled sample.

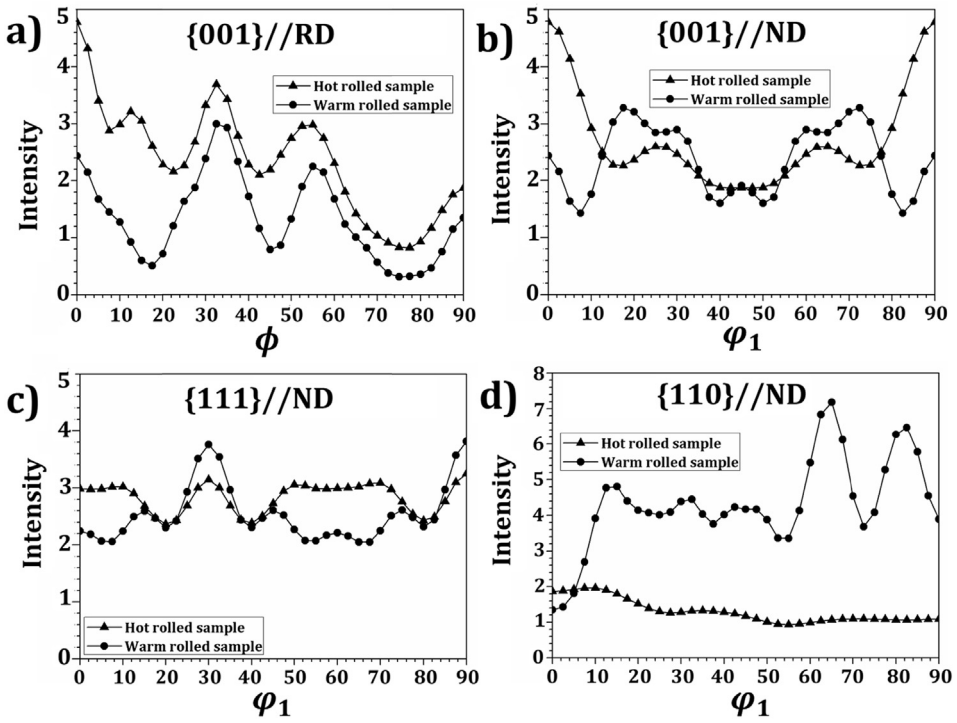

Fig. 5 – Skeleton plots for main fibres a) {001}//RD, b) {001}//ND, c) {111}//ND, d) {110}//ND in hot and warm rolled sample.

HAGBs (point-to-point misorientations greater than 15°) are shown as thin and thick black lines, respectively. In work [7–9] was demonstrated that the hydrogen-induced cracks tend to nucleate and propagate along the grains associated with {001}//ND cleavage planes. This is in good agreement with EBSD result in the vicinity of crack in the hot rolled sample. The IPF colour coding system illustrates a simple way to distinguish the grain orientations. For instance, the grains oriented along {001}, {110} and {111} parallel to the normal direction are indicated in red, green and blue, respectively. The IPF map (Fig. 7a) shows that hydrogen cracks mainly propagated through red grains related to {001}//ND cleavage planes, which is in agreement with previous studies [13–15]. It is well known that the grains oriented with the {110} crystallographic planes correspond to close-packed planes, which can facilitate dislocation movements inside the grains, and can decrease crack growth rate [24]. Local stress concentrations form in the vicinity of boundaries associated with the {001} grains which facilitates crack growth and propagation [25,26].

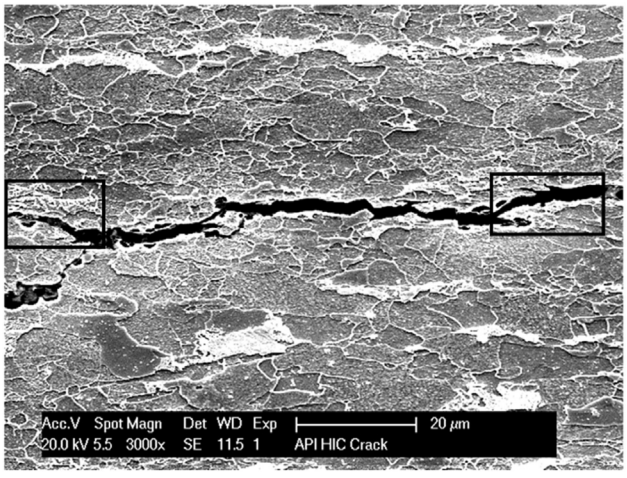

Fig. 6 – Crack propagation after electrochemical hydrogen charging test in hot rolled sample.

The EBSD technique enables to acquire detailed information on individual grains and to determine their deformation degree. To characterise type of grains, the differences between each lattice orientation in individual grains were calculated. If this lattice misorientation is less than 2° the grain is identified as recrystallised. In this respect, lattice mistorientation between 2° and 7° and greater than 7° are designated substructured and deformed grains, respectively. The distribution of recrystallised, substructured and deformed grains in specimens exhibited different behaviour against HIC. The recrystallised, substructured and deformed grains are shown with blue, yellow and red colour. This is presented in Fig. 7b. Large number of substructured and deformed grains was identified in the vicinity of crack path. These types of grains can increase HIC susceptibility due to their high stored energy which is in line with work of Mohtadi-Bonab et al. [27]. It is notable that cracked nucleated and propagated in the absence of external load applied. However, the residual stress generated by previous deformation can contribute to crack extension. Venegas et al. [28] studied the strain field close the HIC crack path in API X46 by variation of EBSD quality patterns. Intense strain fields were localised at the vicinity of crack path which can contribute to increased plastic deformation in this region and consequently enhance crack extension.

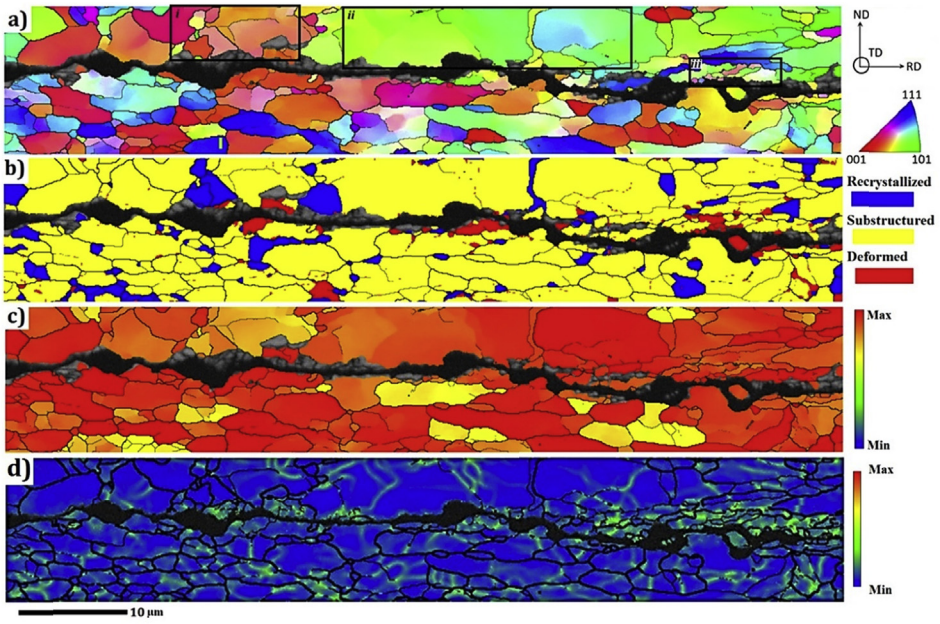

Fig. 7 – The EBSD analysis in the vicinity of HIC, a) IPF map, b) grains type map, c) Taylor factor map and d) strain distribution map.

Taylor factor analysis can predict the level of stress state induced into the grains, which is based on the family of active slip systems [29]. In this study, Taylor factor was calculated using the family of active slip systems for BCC metals {110}<111> and the plane strain deformation [30]. Fig. 7c shows the correlation between grain orientation and crack interaction, such as cleavage planes and slip systems. The grains already aligned to the slip direction are shown in blue, while those with high resistance to yielding are in red. The crack propagated along grains with high Taylor factor values. Grains with high Taylor factor are susceptible to crack propagation as shown in Fig. 7c. In contrary, grains with low Taylor factor (Fig. 9c) were identified in the sample rolled at 850 °C and in this sample no HIC cracks developed after hydrogen charging. Our results are in agreement with those reported by Merriman et al. [31] where grains with a high Taylor factor tend to initiate crack formation due to the dislocation accumulation.

In order to find a correlation between grain orientation and grain size on HIC behaviour, grains located at the upper area of the crack were divided into three regions (Fig. 7a). To determine the exact grain orientation of boxed region (i) in Fig. 7a the ODF was calculated and shown in Fig. 8a. Grains oriented with the (001)<130> components with an orientation within 15° of the ideal cube component with low cleavage resistance is considered as a main crack propagation path. Moreover, in-situ synchrotron X-ray diffraction analysis during tensile loading revealed that {001} crystallographic planes accumulate higher magnitude of lattice strain in comparison to {111} planes [32] which can facilitate crack propagation along {001} grains. Furthermore, an ODF was calculated in the section (ii) at the top of the crack path and presented in Fig. 8b. Grains with 15° deflection from the ideal Goss component were identified. In general, the Goss texture initially forms during hot rolling, and then large grains develop during secondary recrystallization

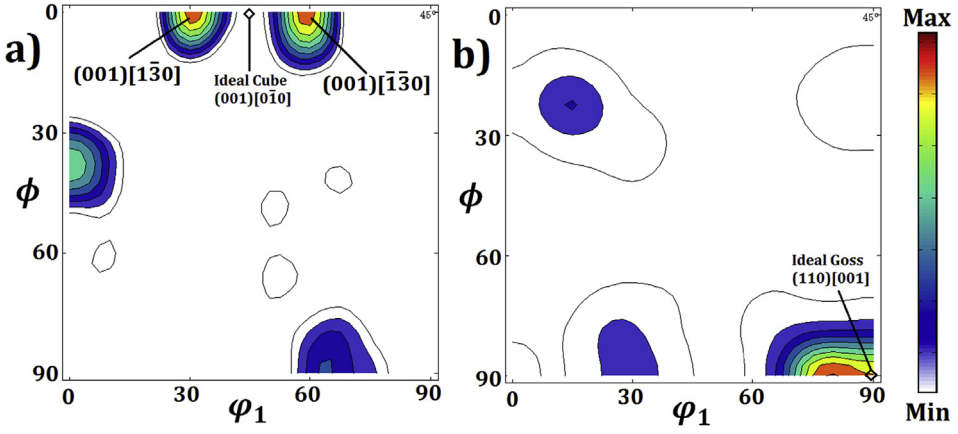

Fig. 8 – Calculated orientation distribution function at $\varphi_2 = 45°$ from a) region i, and b) region ii.

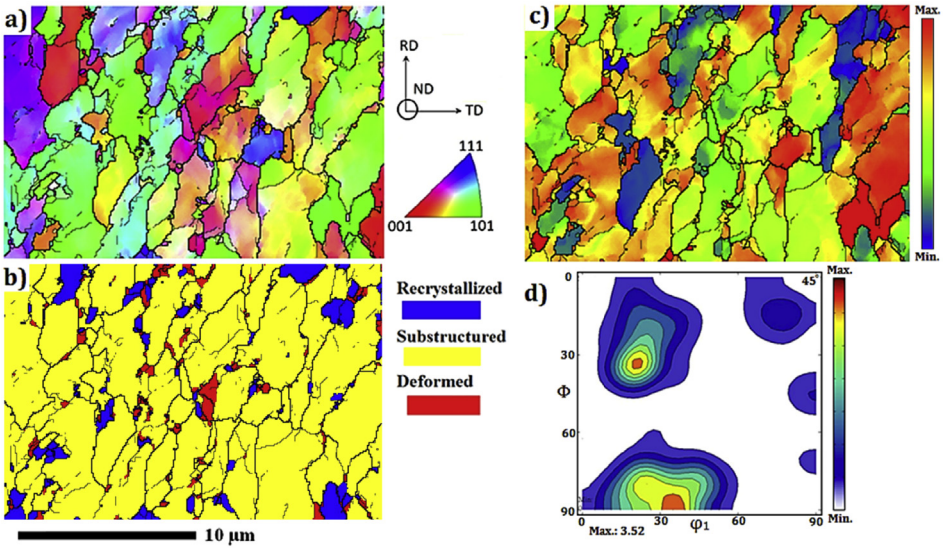

Fig. 9 – The EBSD analysis of warm rolled sample after electrochemical hydrogen charging test, a) IPF map, b) Taylor factor map, c) grains types and d) ODF.

which cause deterioration in mechanical properties [33]. Therefore, Goss texture facilitates crack propagation as observed in Fig. 8b. Finally, the presence of very fine grains near the crack in section (iii) requires more attention. It is known that HIC form when trapped hydrogen reaches the critical amount for crack initiation [19]. Non-metallic inclusions, precipitates, grain boundaries and dislocations are considered as the main trap sites [34,35]. Oudriss et al. [36] also reported that high angle boundaries accommodated by dislocations are capable of hydrogen trapping. Strain distribution map at the vicinity of crack is presented in Fig. 7d. The figure revealed that small grains with large grain boundary surface area accumulate more strain. The larger grain boundary surface area is capable to increase concentration of trapped hydrogen and increase internal pressure by recombination of trapped nascent hydrogen which can boost HIC susceptibility.

As mentioned earlier, no hydrogen-induced crack was found in the sample rolled isothermally at 850 °C. Therefore, EBSD analysis was conducted after the electromechanical hydrogen charging test to investigate the effect of crystallographic orientation on HIC resistance, shown in Fig. 9a. The Taylor factor distributions are presented in Fig. 9b in the same region. A significant low Taylor factor grain distribution was found. This suggests that the lower level of deformation was induced in this condition, due to the possibility of dislocation motions across grains increasing the HIC resistance. Ma et al. [37] reported that the average misorientation angle in {001} grains only reaches 15–30°. Meanwhile, grains oriented with {110} and {112}//ND tend to increase the misorientation angle to 30–60°, leading to sufficient driving force to facilitate the nucleation of recrystallised grains. In this respect, the low number of deformed grains (about 6%) beside finely recrystallised grain distributions in the microstructure (Fig. 9c), enhanced HIC resistance through decreasing of the stored energy. Finally, detailed crystallographic orientation analysis was provided by ODF, and is shown in Fig. 9d. The dominant (112)[2$\bar{4}$ 1] and (110)[1$\bar{1}$ 1] texture components were found, whose planes are parallel to main slip plane in the BCC lattice. According to Humphreys and Hatherly [25], slip occurs in the close-packed <111> directions, but the slip plane could be any of the {110}, {112} or {123} planes. This facilitates dislocation motion across activated slip systems under the electrochemical hydrogen charging test to reduce internal energy and improve resistance to HIC.

Furthermore, the influence of grain boundary distributions on HIC behaviour in both samples after the electrochemical hydrogen charging tests was investigated. Fig. 10 presents the grain boundary distributions including the proportion of LAGBs, HAGBs and coincidence site lattice (CSL) boundaries in both samples. The results showed that the volume fraction of HAGBs and CLS boundaries was higher in the cracked sample, while the proportion of LAGBs was greater in the non-cracked sample. This suggests that hydrogen-induced crack propagation mainly occurs along HAGBs with higher internal energy, while LAGBs, due to the better fit between neighbouring grains, retard crack propagation. Although a small fraction of CSL

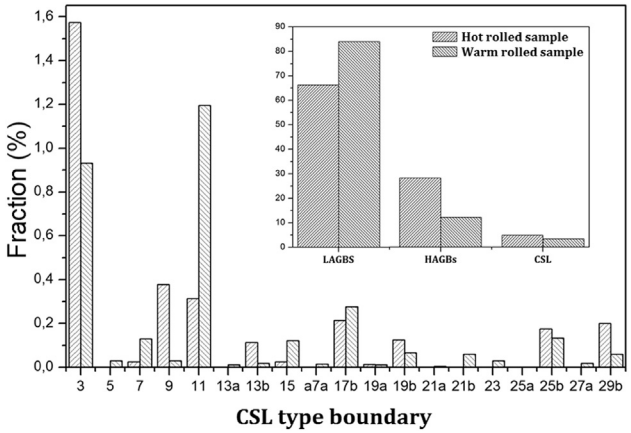

Fig. 10 – Grain boundary distributions in both hot and warm rolled sample.

boundaries was characterised in both samples, it is believed that special boundaries (CSL) with lower stored energy rather HAGBs provide a resistance to crack paths ahead of the crack tip [38]. However, the results were in contrast to hypothesis [37]. Thus, detailed CSL grain boundary distributions are illustrated as well. The number of $\sum 3$ and 9 grain boundary types were higher in the cracked sample, while the fraction of $\sum 11$ was significantly greater in the non-cracked sample. Although $\sum 3^n$ boundaries are considered as twin boundaries, Szpunar et al. [39] reported that in low carbon steel, twining cannot be created due to high stacking-fault energy (SFE). Therefore, these act as HAGBs and enhance crack propagation, leading to greater HIC susceptibility. Conversely, the $\sum 11$ boundaries with a tilt of 50.48° related to <110> plane [40] in the non-cracked specimen was about four times greater than for the cracked sample. Experimental data obtained in this study can be used for complex numerical models [41,42].

Conclusions

Hydrogen-induced crack and electrochemical hydrogen charging tests were carried out in two API X70 pipeline steel samples: industrially rolled at around 1200 °C and rolled isothermally at 850 °C, to investigate the effect of microstructure and crystallographic orientation on hydrogen-induced cracking resistance. The sample rolled isothermally at 850 °C presented a higher HIC resistance in comparison to commercially processed material. The isothermal rolling at 850 °C led to development of sharp {110}//ND texture component accompanied by negligible volume fraction of {001} oriented grains. It was also shown that the grain boundaries associated with {111} and {110} planes can improve HIC resistance. The key finding of this work revealed that significant improvement of HIC resistance was obtained through engineering of crystallographic texture by isothermal rolling at approximately 850 °C. Although the rolling schedule suggested in the current study differs from the established industrial production, a significant improvement in HIC resistance by controlling of texture only was achieved. This can be a great motivation for development of an alternative thermomechanical treatment with lower finish rolling temperature.

Acknowledgement

The authors acknowledge the Brazilian research agencies CNPq and CAPES, the research board of the Federal University of Ceará for the financial support and Laboratory of Electrochemical processes (LabH2S PMT- University of São Paulo), Laboratório de Caracterização de Materiais (LACAM) and Central Analytical (CT-INFRA/MCTI-SISNAD) for the provision of research facilities used in this work.

REFERENCES

[1] Fallahmohammadi E, Bolzoni F, Fumagalli G, Re G, Benassi G, Lazzari L. Hydrogen diffusion into three metallurgical microstructures of a C–Mn X65 and low alloy F22 sour service steel pipelines. Int J Hydrogen Energ 2014;39:13300–13.

[2] Traidia A, Alfano M, Lubineau G, Duval S, Sherik A. An effective finite element model for the prediction of hydrogen induced cracking in steel pipelines. Int J Hydrogen Energ 2012;37:16214–30.

[3] Dong CF, Liu ZY, Li XG, Cheng YF. Effects of hydrogen-charging on the susceptibility of X100 pipeline steel to hydrogen-induced cracking. Int J Hydrogen Energ 2009;34:9879–84.

[4] Serna S, Martínez H, López SY, González-Rodríguez JG, Albarrán JL. Electrochemical technique applied to evaluate the hydrogen permeability in microalloyed steels. Int J Hydrogen Energ 2005;30:1333–8.

[5] Bueno AHS, Moreira ED, Gomes JACP. Evaluation of stress corrosion cracking and hydrogen embrittlement in an API grade steel. Eng Fail Anal 2014;36:423–31.

[6] Nayak SS, Misra RDK, Hartmann J, Siciliano F, Gray JM. Microstructure and properties of low manganese and niobium containing HIC pipeline steel. Mat Sci Eng A 2008;494:456–63.

[7] Venegas V, Caleyo F, Baudin T, Espina-Hernández JH, Hallen JM. On the role of crystallographic texture in mitigating hydrogen-induced cracking in pipeline steels. Corros Sci 2011;53:4204–12.

[8] Arafin MA, Szpunar JA. A new understanding of intergranular stress corrosion cracking resistance of pipeline steel through grain boundary character and crystallographic texture studies. Corros Sci 2009;51:119–28.

[9] Mohtadi-Bonab MA, Szpunar JA, Basu R, Eskandari M. The mechanism of failure by hydrogen induced cracking in an acidic environment for API 5L X70 pipeline steel. Int J Hydrogen Energ 2015;40:1096–107.

[10] Mohtadi-Bonab MA, Eskandari MM, Rahman KMM, Ouellet R, Szpunar JA. An extensive study of hydrogen-induced cracking susceptibility in an API X60 sour service pipeline steel. Int J Hydrogen Energ 2016;41:4185–97.

[11] Moon J, Choi J, Han SK, Huh S, Kim SJ, Lee CH, et al. Influence of precipitation behavior on mechanical properties and hydrogen induced cracking during tempering of hot-rolled API steel for tubing. Mat Sci Eng A 2016;652:120–6.

[12] Wright IS, Field DP. Recent studies of local texture and its influence on failure. Mat Sci Eng A 1998;257:165–70.

[13] Masoumi M, Herculano LFG, Abreu HFG. Study of texture and microstructure evaluation of steel API 5L X70 under various thermomechanical cycles. Mat Sci Eng A 2015;639:550–8.

[14] Masoumi M, Silva CC, Abreu HFG. Effect of crystallographic orientations on the hydrogen-induced cracking resistance improvement of API 5L X70 pipeline steel under various thermomechanical processing. Corros Sci 2016;111:121–31.

[15] Nafisi S, Arafin MA, Collins L, Szpunar J. Texture and mechanical properties of API X100 steel manufactured under various thermomechanical cycles. Mat Sci Eng A 2012;531:2–11.

[16] Mohtadi-Bonab MA, Szpunar JA, Razavi-Tousi SS. Hydrogen induced cracking susceptibility in different layers of a hot rolled X70 pipeline steel. Int J Hydrogen Energ 2013;38:13831–41.

[17] Mesquita TJ, Chauveau E, Mantel M, Kinsman N, Nogueira RP. Influence of Mo alloying on pitting corrosion of stainless steels used as concrete reinforcement. R Esc Minas, Ouro Preto 2013;66:173–8.

[18] Farahat AIZ. Dilatometry determination of phase transformation temperatures during heating of Nb bearing low carbon steel. J Mater Proces Tech 2008;204:365–9.

[19] Mohtadi-Bonab MA, Szpunar JA, Razavi-Tousi SS. A comparative study of hydrogen induced cracking behavior in

API 5L X60 and X70 pipeline steels. Eng Fail Anal 2013;33:163–75.
[20] ANSI/NACE TM0284-2016, Evaluation of pipeline and pressure vessel steels for resistance to hydrogen-induced cracking.
[21] Zhu LX, He XD, Han XL, Qu TT. Effect of M/A constituents on mechanical properties of high grade pipeline steel. Adv Mat Res 2011;284:1271–4.
[22] Zhang N, Yang P, Mao W. Formation of cube texture affected by neighboring grains in a transverse-directionally aligned columnar-grained electrical steel. Mater Lett 2013;93:363–5.
[23] Mohtadi-Bonab MA, Szpunar JA, Collins L, Stankievech R. Evaluation of hydrogen induced cracking behavior of API X70 pipeline steel at different heat treatments. Int J Hydrogen Energ 2014;39:6076–88.
[24] Humphreys FG, Hatherly M. Recrystallization and related annealing phenomena. 2nd ed. Amsterdam, Boston: Elsevier; 2004. p. 25–9.
[25] Yang W, Lee WB. Grain boundary engineering and related topics. Mesoplasticity and its applications, Mater Res Eng, 361–390.
[26] Pal S, Alam ME, Odette GR, Hoelzer D, Maloy S. Texturing, microcracking and delamination in 14ywt nanostructured ferritic alloys. TMS2016, Materials and Fuels for the Current and Advanced Nuclear Reactors V.
[27] Mohtadi-Bonab MA, Eskandari M, Szpunar JA. Texture, local misorientation, grain boundary and recrystallization fraction in pipeline steels related to hydrogen induced cracking. Mater Sci Eng A 2015;620:97–106.
[28] Venegas V, Caleyo F, González JL, Baudin T, Hallen JM, Penelle R. EBSD study of hydrogen-induced cracking in API-5 L-X46 pipeline steel. Scr Mater 2005;52:147–52.
[29] Taylor GL. Plastic strain in metals. J Inst Met 1938;62:112–24.
[30] Delannay L, Jacques PJ, Kalidindi SR. Finite element modeling of crystal plasticity with grains shaped as truncated octahedrons. Int J Plast 2006;22:1879–98.
[31] Merriman CC, Field DP, Trivedi P. Orientation dependence of dislocation structure evolution during cold rolling of aluminum. Mat Sci Eng A 2008;494:28–35.
[32] Collins DM, Mostafavi M, Todd RE, Connolley T, Wilkinson AJ. A synchrotron X-ray diffraction study of in situ biaxial deformation. Acta Mater 2015;90:46–58.
[33] Jia N, Eisenlohr P, Roters F, Raabe D, Zhao X. Orientation dependence of shear banding in face-centered-cubic single crystals. Acta Mater 2012;60:3415–34.
[34] Sha Q, Li D. Microstructure and properties of low manganese APIx70 pipeline steel for sour service application. In: PRICM: 8 Pacific rim international congress on advanced materials and processing; 2013.
[35] Yazdipour N, Dunne DP, Pereloma EV. Effect of grain size on the hydrogen diffusion process in steel using cellular automaton approach. Mater Sci Forum 2012;706:1568–73.
[36] Oudriss A, Creus J, Bouhattate J, Savall C, Peraudeau B, Feaugas X. The diffusion and trapping of hydrogen along the grain boundaries in polycrystalline nickel. Scripta 2012;66:37–40.
[37] Ma Q, Mao W, Li B, Wang PT, Horstemeyer MF. Grain subdivision and its effect on texture evolution in an aluminum alloy under plane strain compression. TMS Light Met 2013:351–5.
[38] Mahajan S, Pande CS, Imam MA, Rath BB. Formation of annealing twins in f.c.c. crystals. Acta Mater 1997;45:2633–8.
[39] Eskandari M, Yadegari-Dehnavi MR, Zarei-Hanzaki A, Mohtadi-Bonab MA, Basu R, Szpunar JA. In-situ strain localization analysis in low density transformation-twinning induced plasticity steel using digital image correlation. Opt Lasers Eng 2015;67:1–16.
[40] Mykura H. A checklist of cubic coincidence site lattice relations. In: Grain boundary structure and kinetics, asm materials science seminar. Materials Park (OH): ASM International; 1980. p. 445.
[41] Novotný L. Calculation of T–stress on 3D specimens with crack. Procedia Eng 2012;48:489–94.
[42] Halama M, Jerolitsch D, Zilková J, Dzedzina R, Linhardt P. Improvement of ENA-NOCS technique using artificial neural networks approach for the detection of corrosion eurocorr. 2010. p. 1–8.